

Differentiation Between Faults and Cyberattacks through Combined Analysis of Cyberspace Logs and Physical Measurements

Mohammad Shamim Ahsan, Haizhou Wang, Venkateswara Reddy Motakatla, Minghui Zhu, and Peng Liu, *Member, IEEE*

Abstract—In recent years, cyberattacks - along with physical faults - have become an increasing factor causing system failures, especially in DER (Distributed Energy Resources) systems. In addition, according to the literature, a number of faults have been reported to remain undetected. Consequently, unlike anomaly detection works that only identify abnormalities, differentiating undetected faults and cyberattacks is a challenging task. Although several works have studied this problem, they crucially fall short of achieving an accurate distinction due to the reliance on physical laws or physical measurements. To resolve this issue, the industry typically conducts an integrated analysis with physical measurements and cyberspace information. Nevertheless, this industry approach consumes a significant amount of time due to the manual efforts required in the analysis. In this work, we focus on addressing these crucial gaps by proposing a non-trivial approach of distinguishing undetected faults and cyberattacks in DER systems. Specifically, first, a special kind of dependency graph is constructed using a novel virtual physical variable-oriented taint analysis (PVOTA) algorithm. Then, the graph is simplified using an innovative node pruning technique, which is based on a set of context-dependent operations. Next, a set of patterns capturing domain-specific knowledge is derived to bridge the semantic gaps between the cyber and physical sides. Finally, these patterns are matched to the relevant events that occurred during failure incidents, and possible root causes are concluded based on the pattern matching results. In the end, the efficacy of our proposed automatic integrated analysis is evaluated through four case studies covering failure incidents caused by the FDI attack, undetected faults, and memory corruption attacks.

Index Terms—Differentiation, cyberattacks, faults, DER system, cyber physical system

I. INTRODUCTION

DIFFERENTIATION between undetected faults and cyber attacks is a critical issue in DER (Distributed Energy Resources) systems, due to at least two main reasons. First, catastrophic failure incidents (e.g., outages) in modern power systems are no longer entirely caused by system faults: cyber attacks are an increasing factor. For example, (a) the complete blackout in Ukraine due to a large-scale cyber attack [11]; (b)

This work has been submitted to the IEEE Transactions on Smart Grid for possible publication. Copyright may be transferred without notice, after which this version may no longer be accessible.

Mohammad Shamim Ahsan, Haizhou Wang and Peng Liu are with the College of Information Sciences and Technology, Pennsylvania State University, University Park, PA 16801 USA. (email: msa6152@psu.edu, hzw5074@psu.edu, pxi20@psu.edu)

Venkateswara Reddy Motakatla is with the National Renewable Energy Laboratory (NREL), Golden CO, USA. (email: VenkateswaraReddy.Motakatla@nrel.gov)

Minghui Zhu is with the Department of Electrical Engineering, The Pennsylvania State University, University Park, PA 16802 USA (email: muz16@psu.edu)

Manuscript received September xxx, 2025; revised September xxx, 2025.

the Iranian cyberattack on industrial PLCs located in many countries, including multiple US states [3]. Second, many faults in DER systems are *undetected faults*. For example, (a) standard protection devices like fuses and circuit breakers may not be sufficient to detect all types of faults in solar photovoltaic (PV) systems; (b) faults that occur under low irradiation conditions may go undetected; (c) PV arrays can experience multiple faults simultaneously, confusing the fault detectors. Third, if differentiation is ignored, the failure recovery procedure could be seriously affected. For example, system operators may mistakenly conclude that a failure is caused by faults when it is actually caused by a cyber attack. This often leads to ineffective incident response and recovery. Ultimately, the affected system becomes more vulnerable and less resilient [19]. It is widely recognized in the literature that differentiation between undetected faults and cyber attacks is indispensable [18].

A significant number of works in the literature [8], [20], [21] have focused on detecting anomalies (e.g., power outages). But it should be noted that techniques for detecting anomalies and techniques for differentiating between faults and cyber attacks are different in principle. Specifically, these anomaly detection systems (ADSs) can only detect whether something is abnormal, not the specific type of anomaly. Several studies have been conducted on distinguishing undetected faults and cyberattacks [4], [5], [7], [9], [10], [14]–[16]. These works focus on the physical side of CPSs and are based on physical laws or physical measurements. Unfortunately, reliance on physical laws makes these works limited to effectively handle real-world signal noise [13], and the reliance (e.g., take a machine learning approach) on physical measurements is prone to suffering from inaccuracy due to the imbalanced data in CPS [12] and from limited explainability. To mitigate these issues, the DER industry utilizes the analysis results of the existing detection and differentiation techniques, but does **not** treat them as the final outcome. Rather, a team of human analysts is synthesizing the various intermediate analysis results to integrate the findings from not only physical side analyzers (e.g., ADSs, localization analyzers) but also cyberspace analyzers (e.g., data dependency analyzers). A main goal is to integrate physical and cyberspace information (e.g., obtained through taint analysis) to avoid severe consequences caused by incorrect cause identification. Specifically, cyberspace uniquely contains some critical information, especially a variety of logs and data dependencies that can facilitate the task of correctly differentiating undetected faults and various cyberattacks.

However, the industry approach is very time-consuming, as

it involves a lot of manual effort. In this paper, we propose an approach to take the first step towards automatically synthesizing physical side and cyberspace findings. The mapping relationships shown in Figure 1 provide a fundamental reason why combined analysis could create a unique capability. In this figure, the mapping relationships on the top of the figure are between the virtual physical variables (from which physical side measurements are collected) and the program variables used by DERMS (DER Management System) applications, and the mapping relationships on the bottom of the figure are between the program variables used by DERMS applications and physical side control of DER. Note that the messages sent from DERMS applications to DER devices play an essential role in achieving control of DER. Specifically, if taint propagation (i.e., information flow from one entity to another) is observed in the cyberspace from a variable that is mapped to a physical side measurement to a variable that is mapped to a physical side control, then the extended cyber-physical taint propagation would provide a unique lens to examine not only the (varied) effects of different cyberattacks, but also the differences between undetected faults and cyberattacks. Although this kind of mapping is highly desirable, it is non-trivial to achieve due to the following challenge: existing automatic taint analysis techniques [6], [17] fall short of meeting the synthesized analysis requirements of a DER system. On one hand, forward taint analysis explicitly requires both the taint source (i.e., a particular program variable that appears in a specific line of code) and the sink in advance. However, the incident report used by analysts, though it contains a detailed description of the detected anomalies, usually does not tell what the specific taint sources are. On the other hand, backward taint analysis identifies all the possible taint sources for a given sink, but most of the identified sources are usually irrelevant to the reported incident, and examining them can waste a considerable amount of resources. Moreover, currently, the connections between physical measurements and cyberspace information items (e.g., data dependencies between program variables) are not being automatically analyzed in real-world practice. In fact, significant semantic gaps exist between physical measurements and cyberspace information items.

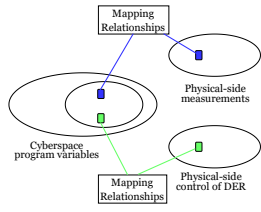


Fig. 1. Mapping between cyberspace program variables and physical system variables in a DER system

To address these challenges, we develop two new ideas. First, a virtual physical variable-oriented taint analysis (*PVOTA*) algorithm is introduced, where the virtual physical variable(s) mentioned in the incident report is used to guide our analyzer to automatically find corresponding tainted sources and taint propagation paths. Second, a set of patterns

is designed, where each pattern is devised to help bridge the semantic gap between physical side measurements and cyberspace information. These two ideas make our proposed approach non-trivial. In particular, a special kind of dependency graph is constructed based on the first idea of *PVOTA*. Specifically, we start with virtual physical variable(s): first, a backtracking mechanism along with a heuristic is employed to find the taint sources; second, a forward tracking mechanism is utilized to identify the taint propagation paths that reach the sink. Then, a set of context-dependent operations is performed to prune the less important nodes from the graph. Assisted by the constructed simplified dependency graph, a set of specific patterns is leveraged to cross-check the observed physical-side and cyberspace information items, and we audit the matched patterns. After that, the matching results are synthesized to conclude about the root cause of the failure incident. The proposed approach makes the differentiating task much more time-efficient than the current industry approach. Accordingly, manual efforts, and hence the required time, are substantially reduced. In summary, the following contributions are made in this work:

- A virtual physical variable-oriented taint analysis (*PVOTA*) technique is proposed to construct dependency graphs, especially in DER systems.
- A set of patterns is derived to bridge the semantic gap between the cyber and physical sides. Assisted by the dependency graphs constructed by the *PVOTA* technique, we match these patterns against the relevant events that had happened during each reported incident, and a decision on the root cause is made by observing the pattern-matching results.
- To evaluate the feasibility and efficacy of the proposed combined analysis approach, we conduct several case studies that cover three representative types of incidents: an incident caused by a False Data Injection attack, an incident caused by undetected faults, and an incident caused by a memory corruption attack.

II. BACKGROUND AND EXISTING WORKS

A. DER Systems and Cyberattacks

Typically, a DERMS application is used by utilities to manage diverse and dispersed DERs, both individually and in aggregate. From the lowest level, different services of the DERs (e.g., individual EVs, rooftop PVs, household batteries, etc.) or microgrids are coordinated and scheduled by a flexible resource scheduler (FRS), which operates as a local DERMS for its substation. Both utility-scale and behind-the-meter DERs can be managed either directly by the FRS or through a transactive market manager (TMM) or DER aggregators. In either case, a DERMS application is used to dispatch DER resources and real-time control. The next two upper layers of a DERMS are the DSO (Distributed System Operator) and the TSO (Transmission System Operator), which coordinate and manage signals from all substations to provide distribution and transmission services.

The distributed nature and complex interconnectivity of DERMS make it vulnerable to cyberattacks, particularly false

data injection (FDI), memory corruption, and man-in-the-middle (MITM) attacks. In an FDI attack, the attacker tries to manipulate DER operations by injecting falsified data of various types. Considering the distributed architecture of DERMS, any erroneous data injected into the communication layer can result in a cascading effect on the DERs that affects grid stability, control operations, and normal voltage or current flows. In an MITM attack, the attacker intercepts or modifies critical data by compromising a gateway, a router, communication channels, or other non-end equipment. During a memory corruption attack, the attacker exploits the vulnerability of DERMS application program executions by overwriting or overflowing different memory segments, notably the stack and heap.

B. Undetected Faults in PV Systems

In photovoltaic (PV) systems, ground faults, arc faults, and line-to-line faults are identified as major causes of catastrophic failures [2]. Regarding protection devices, ground fault detection and interruption fuse (GFDI) protects equipment from being affected by a significant current flow to the ground circuit caused by an accidental connection between a current-carrying conductor (CCC) and an equipment grounding conductor (EGC) or earth [2]. However, the leakage current can return to the PV conduction path through these fuses, which is an unintentional systematic drawback of this device. Arc-fault circuit interrupter (AFCI) is another protection device that protects PV arrays from being fire hazards caused due to the discontinuities in the CCCs or insulation breakdown in adjacent CCCs. To handle line-to-line faults, overcurrent protection devices (OCPDs) are used when the fault current is higher than the rated current of OCPD, which is at most 1.56 times the short-circuit current [22]. However, these faults may remain undetected when they occur under low irradiance since the current is not large enough to melt the OCPD [22].

C. Taint Analysis

Taint analysis is a program analysis technique that tracks the information flow originating from untrusted sources (e.g., API functions, user inputs), which propagates along the program execution path and eventually reaches release points or sensitive functions (known as *sinks*). Data entered into the program by these sources is considered *tainted*, thereby causing all dependent variables to be tainted as well. An example of such propagation can be described using the code statements: `x=get_input(); y=1; z=x; w=y+z;`, where `get_input()` is a taint source, as untrusted data can enter the program through it. Consequently, `x` becomes tainted. However, `y` is untainted as it allocates a constant value. Since `z` has data dependency on `x`, it becomes tainted as well. According to the taint propagation rule: *tainted+untainted=tainted*, `w` is also considered tainted. Due to these data dependencies in programs, an attacker can exploit taint sources to manipulate inputs and critical computations, and taint analysis can effectively trace the propagation paths of such tainted data through the program.

D. Related Works

Although works on differentiating faults and attacks are comparatively less than that of detecting, existing research can be categorized into two groups: physical law-based and physical side measurements-driven.

In the first group, approaches depend on the physical laws or mathematical foundations of system design and typically make a set of assumptions prior to modeling. Optimization-based frequency-domain approach [4], mapping of physics law-driven trajectories on a frequency-active voltage-centric Cartesian plane [10], asymmetric relationship-based approach for analyzing compromised frequency signals [14], residual signals construction using an adaptive sliding mode observer technique [5] are the most prominent systems in the literature. Regarding physical side measurement-driven approaches, they predict based on real-time and historical power measurements. Sakhini et al. [15] classify attacks and faults with localization to particular measurements in the operational layer (a.k.a. physical layer) of smart grids using an ensemble algorithm and data representation learning. A deep neural network (DNN)-based strategy is proposed in [9] using historical outage data received from protection relays (both feeder and DER) and fault indicators to classify physical faults and different cyberattacks, including FDI and replay attacks. Other well-known strategies utilize parametric time-frequency logic (PTFL) [7], multi-label CNN with matrix singular value decomposition (SVD) [16], etc.

Limitations. The primary limitation of physical law-based approaches is the inefficiency of handling real-world signal noise [13]. In addition, these models are often constrained by a predefined set of assumptions (e.g., losslessness of the system, dependency on frequency-specific synchronized PMU measurements), which may limit their applicability in some situations. With regard to approaches that rely on physical side measurements, the fundamentally crucial issue is the quality of the train-test datasets. In most cases, an imbalanced data distribution is observed in various fault and attack classes, severely affecting these approaches, especially supervised machine learning-based models [12]. One convincing reason behind this is the scarcity of anomalous data, since system failure incidents are not particularly frequent. Moreover, these physical measurement-driven approaches are also difficult to explain.

III. PROPOSED APPROACH

A. Problem Statement

How to automatically conduct a combined analysis to achieve differentiation between undetected faults and cyber-attacks? By combined analysis, we mean the following: if taint propagation is observed in the cyberspace from a DERMS application program variable that is mapped to a physical side measurement to a variable that is mapped to a physical side control, then the extended cyber-physical taint propagation would provide a unique lens to examine the differences between undetected faults and cyber-attacks. It should be noticed that the techniques for detecting anomalies

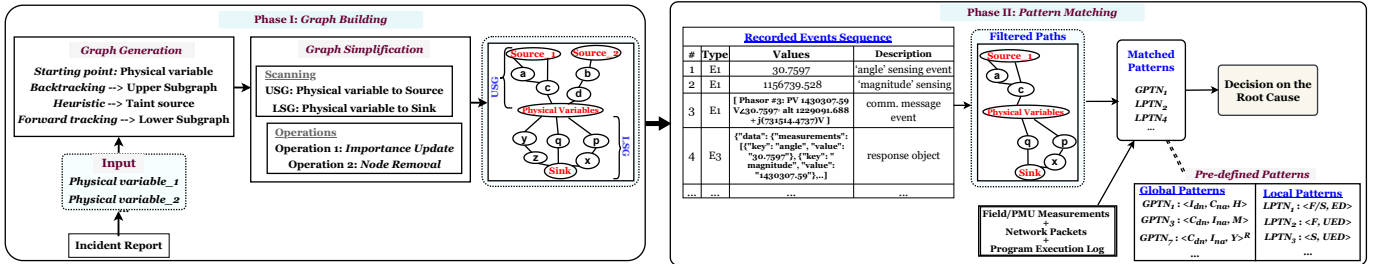


Fig. 2. Overview of the proposed approach

and the techniques for differentiating between faults and cyber-attacks are *inherently* different. An ADS detects anomalies, but does not differentiate between the *causes* for the detected anomaly.

Definitions. We define a new term, *virtual physical variable*, which represents a DERMS application program variable that is used to hold the value of physical side measurements. In addition, the set of virtual physical variables, taint sources, and sinks are represented by P_{var} , T_{src} , and T_{snk} , respectively. Moreover, a variable is considered as an *auxiliary variable*, denoted as V_s , if it is neither a virtual physical variable, a function call, nor an array/object related variable.

B. Overview

In this paper, we propose a novel approach to distinguish undetected faults and cyberattacks utilizing both physical-side measurements and cyberspace information. In particular, a virtual physical variable-oriented taint analysis technique, *PVOTA* is introduced to generate dependency graphs, and a set of domain-specific patterns is derived from the physical side and cyberspace information to capture distinct characteristics of individual causes. Specifically, the proposed approach consists of two main phases: graph building and pattern matching, as illustrated in Figure 2. In the graph builder component, at first, virtual physical variable(s) are collected from the incident report. Next, two dependency subgraphs - upper subgraph (*USG*) and lower subgraph (*LSG*) - are constructed based on these variables using backward taint tracking and forward taint tracking, respectively. After that, a new algorithm is developed to remove less important nodes from the subgraphs using a set of context-dependent operations. At the beginning of the pattern-matching phase, incident-related paths in the *USG* and the *LSG* are selected based on a sequence of events recorded during the system failure. Then, each node of these paths is traversed to find matched patterns to determine the root cause. In the following two subsections, each component is explained in detail.

1 Phase I: Graph Building. This is the first phase of our proposed approach that comprises two steps: graph generation and graph simplification. In the first stage, a specialized dependency graph is constructed using a non-trivial taint analysis technique. In the subsequent stage, a

novel graph pruning strategy is employed to retain only the most relevant nodes in the graph.

C. Graph Generation Technique

To investigate the root cause of system failures based on both physical-side measurements and cyberspace information, such as server application code, network packets, and DERMS application logs, it is arguably essential to identify entry points, precise propagation paths, and the exit point that has affected related DER devices. This observation initiates the necessity of employing a taint analysis technique, where taint propagation is observed from a given source to the distinguished sink. However, standard taint analysis is not appropriate, especially for DER systems. One of the major issues is that not all generated tainted paths are related to causing system failure; only those that include virtual physical variables are relevant since real-world is affected by the alteration of their measurements. For example, for the graph illustrated in Figure 3, almost half of the tainted paths generated by a standard taint propagation technique are irrelevant to the root cause analysis, specifically for the cyber-physical system (CPS) domain. Another shortcoming of standard taint analysis is the requirement of having prior knowledge of the sources and sinks, which is not always feasible. In contrast, our proposed approach adopts a taint analysis method and overcomes these limitations by utilizing a forward and backward propagating strategy to generate tainted paths started from virtual physical variables, along with a heuristic to determine the potential tainted sources.

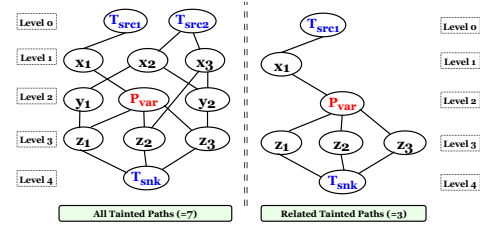


Fig. 3. An example to demonstrate the shortcomings of the traditional taint analysis technique

Approach. At the beginning of the graph construction, we start with $P_{var_i} \in P_{var}$ and propagate upward using a backtracking approach to generate *Upper Subgraph* (*USG*). Since during backtracking, the taint sources

and their volume are unknown, a heuristic is proposed to find potential taint sources. Specifically, two API calls: `GridAPPSD(username, password)` and `conn.get_response(t.TIMESERIES, message)` are identified as tainted sources during the case studies conducted later.

At the beginning of the heuristic, two observations are made: i) a user-defined function can never be a taint source, and ii) typically, taint sources include API calls, command line argument handling functions, query processing functions, and different types of read functions. Then, a node-weighting strategy is employed in the generated *USG* to find the set of taint sources (T_{src}). Specifically, during backtracking, we assign weight W_k to each node N_k as follows: $W_k = 1$ if $N_k \in P_{var}$; $W_k = W_k + 1$ if $N_k \in T_{src}$; and $W_k = W_k + \frac{1}{2}$ otherwise. Finally, while forward tracking through each path, start from a node that does not have any outgoing edge, and keep removing nodes until a node is found with two characteristics: i) $W_k \geq 1$ and ii) any feature from the possible taint sources. Whenever such a node is found, the process is stopped.

Next, a forward traversal technique is applied to construct the *Lower Subgraph* (*LSG*), which begins at P_{var_i} and ends whenever any $T_{snk_i} \in T_{snk}$ is found. Each node contains the specific tainted entity in the program. A tainted entity can be either an identifier (e.g., variable, object, referencing, expression) or a function call. On the other hand, similar to the classic taint propagation technique, our proposed technique leverages directed edges that represent generic dependency. Specifically, an edge from node a to node b is denoted as $E(a, b)$. During forward traversal, this edge indicates propagation of taint from a to b . However, while backtracking, the tainted data flows in the opposite direction, from b to a for the edge $E(a, b)$. The back-front traversal is similar to the standard taint analysis technique. However, regarding propagating through functions, the following modifications have been made to the rules:

- I. During backtracking, propagate from each argument. If an argument is related to an object, then propagate the object. Additionally, if the function is bound to any object, then consider the object too. For inter-procedural flows, start backtracking from the `return` statement. Figure 4 illustrates these scenarios, and Figure 5 presents a code example of an inter-procedural flow.
- II. While approaching forward, do not propagate the argument variables of the API calls, command line arguments functions, query functions, or any kind of input functions; rather, continue from the variables from which their values are assigned. To handle calls across functions, propagate through the tainted parameters located inside the callee function. For instance, let x, y, z be the arguments of a function `myFunc(x, y, z)` and only x is tainted. Therefore, the propagation will continue through x located at the definition of this function.
- III. *Special case:* Handling *callback functions* is as a special case since they are not directly called and always related to any object of a defined class. For example, `_on_message()` is a callback function in DERMS

that is automatically called whenever there is a message in the system. One way to tackle them is to propagate from the already tainted variables of that object. Usually, a *callback function* can only be found during forward tracking, that is, after the virtual physical variables are fed some values.

However, to avoid complications, we ignore the case where a traversing function is called by another function (a.k.a., indirect connection) as shown in Figure 6.

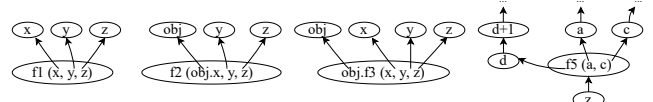


Fig. 4. Handling propagation through function during backtracking

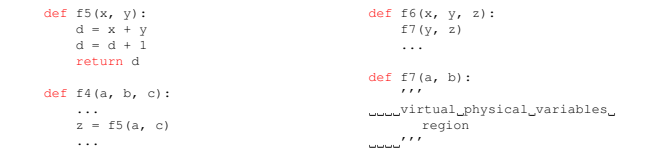


Fig. 5. An Inter-procedural Flow. Fig. 6. An Indirect Connection.

Graph Simplification Technique. To increase the readability and usability of the generated graphs, we develop a non-trivial simplification algorithm, where less significant nodes are eliminated using several context-based operations. The detailed technique can be found in the [technical report](#) [1].

2 Phase II: Pattern Matching. Usually, taint propagates through events, and these events are recorded in the tainted paths, which can be related or unrelated to the root cause of the incident. Based on this observation, the proposed pattern-matching technique starts with the selection of incident-related paths from the dependency graph constructed in Phase I. Specifically, a human analyst filters out unrelated paths using a sequence of events recorded during the incident. Examples of such sequences can be found in the next section (Section IV). It is worth mentioning that these sequences are unique to each incident, and selecting relevant paths requires domain-specific knowledge that the human analyst has. In the subsequent step, each node in the filtered path(s) is traversed, and different logs are examined to identify potential matches based on the predefined patterns. In this section, we introduce a set of patterns to bridge the semantic gap between cyberspace and the physical side. Since the proposed decision-making strategy requires specific incident-related information, the entire process is described in the case studies.

D. Patterns

In our proposed approach, the predefined patterns utilize three types of information: (i) data files holding PMU measurements (referred to as field measurements), (ii) Network packets PCAP (packet capture) files used to monitor network activities, and (iii) DERMS application log generated during the execution of the application program. Each variable in these logs is represented as a tuple: $\langle t, v \rangle$, where t and v denote the timestamp and value of the variable. In addition,

$\langle t_x^d, v_x^d \rangle$, $\langle t_x^n, v_x^n \rangle$, and $\langle t_x^a, v_x^a \rangle$ are used to represent tuples for variable ‘ x ’ in the corresponding logs. In a DER system, a dependency graph typically consists of three types of nodes: response message-related, dispatch message-related, and other program variables-related. However, for only response and dispatch messages, corresponding field measurements and network packets exist. In accordance with this knowledge, a set of patterns, referred to as *global patterns* is devised to match abnormal system-wide event sequences. On the other hand, for other program variables that are only recorded in the application log, a separate set of patterns, called *local patterns*, is used to track their values. Although global patterns are explicitly based on the time order, the constructed graph implicitly carries the time order of the executed program.

1) *Global Patterns*: These patterns are developed to analyze the response and dispatch-related information available in every log. To monitor consistency between the log files, four new notations are introduced. In particular, I_{dn} and C_{dn} indicate inconsistency ($v_x^d \neq v_x^n$) and consistency ($v_x^d = v_x^n$), respectively, between the field measurements and the network packet. Likewise, I_{na} and C_{na} indicate inconsistency ($v_x^n \neq v_x^a$) and consistency ($v_x^n = v_x^a$), respectively, between the network packet and the application log. In addition, the orders of timestamps are $t_x^d < t_x^n < t_x^a$ and $t_x^d > t_x^n > t_x^a$ for response and dispatch, respectively. Here, two different time-orderings indicate the opposite directions of data flows during response (physical side \rightarrow cyberspace) and dispatching (cyberspace \rightarrow physical side). Typically, the value of any information, irrespective of a field measurement, network packet field, or program variable, can be a float or a string, depending on its content. These observed values are compared with the normal (‘benign’) ones to measure the *deviation*. For a float-type variable, first, a histogram is plotted using the historical ‘benign’ values of that variable. Let the total number of measurements and the total number of bins be n and m , respectively. Moreover, the bins are $B_1, B_2, B_3, \dots, B_m$ and the corresponding number of measurements in these bins are $n_1, n_2, n_3, \dots, n_m$. Now, the value is considered to be *deviated* if it cannot be located in any bin or is located in one of the smaller bins (say, bin B_i and the relative size $p_i = n_i/n$ is too small). However, for string-type variables, such statistical analysis is not needed since their values usually remain fixed in ‘benign’ incidents. For either case, the existence and non-existence of deviation is denoted as Y and N , respectively. Based on this strategy, each global pattern is represented as $GPTN_k \equiv \langle I_{dn}/C_{dn}, I_{na}/C_{na}, Y/N \rangle$. Eight such useful patterns are listed in Table I.

2) *Local Patterns*: These patterns enable us to monitor potential deviations in each node of the graph using the DERMS application log. To represent the degree of deviation, a new notation Δ (Delta) is introduced. For a float-type node, Δ can be low (L), moderate (M), or high (H); whereas, for a string-type node, it is always considered high (H). The decision on Δ can be taken using the same histogram approach described in the global patterns section. Specifically, Δ is inversely proportional to p_i . The lower the p_i , the higher the likelihood of being considered as H; and vice versa. In any case, if the observed value cannot be assigned to any bin, then

TABLE I
LIST OF PATTERNS. $GPTN_1 - GPTN_8$ ARE THE GLOBAL PATTERNS AND $LPTN_1 - LPTN_5$ ARE THE LOCAL PATTERNS. [$Y \equiv$ DEVIATION EXISTS, $N \equiv$ DEVIATION DOES NOT EXIST, $F \equiv$ FLOAT, $S \equiv$ STRING, $ED \equiv$ EXPECTED DEVIATION, $UED \equiv$ UNEXPECTED DEVIATION, $\top \equiv$ UNKNOWN, $R \equiv$ DISPATCH-SPECIFIC GLOBAL PATTERNS]

Pattern #	Definitions	Interpretation
$GPTN_1$	$\langle I_{dn}, C_{na}, Y \rangle$	inconsistent network packet, deviation exists
$GPTN_2$	$\langle I_{dn}, C_{na}, N \rangle$	inconsistent network packet, deviation does not exist
$GPTN_3$	$\langle C_{dn}, I_{na}, Y \rangle$	inconsistent application log, deviation exists
$GPTN_4$	$\langle C_{dn}, I_{na}, N \rangle$	inconsistent application log, deviation does not exist
$GPTN_5$	$\langle C_{dn}, C_{na}, Y \rangle$	logs are consistent, deviation exists in field measurements
$GPTN_6$	$\langle C_{dn}, C_{na}, N \rangle$	logs are consistent, no deviation in field measurements
$GPTN_7$	$\langle C_{dn}, I_{na}, Y \rangle^R$	inconsistent network packet, deviation exists
$GPTN_8$	$\langle C_{dn}, I_{na}, N \rangle^R$	inconsistent network packet, deviation does not exist
$LPTN_1$	$\langle F/S, ED \rangle$	expected deviation exists
$LPTN_2$	$\langle F, UED \rangle$	unexpected deviation exists for float node
$LPTN_3$	$\langle S, UED \rangle$	unexpected deviation exists for string node
$LPTN_4$	$\langle F/S, \top \rangle$	log not available, or no deviation exists in the node
$LPTN_5$	$\langle Others, \top \rangle$	function call or object (needed to maintain analytical flow)

Δ is considered H. Here, this measurement is intentionally kept as abstract (i.e., low, moderate, and high) to support a customization facility for the security analyst. In addition, the degree of deviation is also system-dependent. For further analysis, two new concepts: *expected deviation* and *unexpected deviation* are defined, which represent what kind of behavior is expected to be observed at every node in the graph. If the degree of deviation at node X is Δ_X and node Y is a dependent of X , then the expected deviation in Y is referred to as $\Delta_X \rightarrow \Delta_Y$ and the unexpected deviation is denoted by $\Delta_X \rightarrow \Delta'_Y$. The presence of Δ'_Y emphasizes the possibility of a memory corruption attack in that node or any of its predecessor nodes. However, the existence of Δ_Y does not necessarily indicate any root cause; rather, it implies the need for continued analysis. Ideally, the ‘benign’ values related to node Y are available, and Δ_Y can be calculated using the proposed histogram approach. However, in practice, only a set of program variables is logged into the system. As a consequence, the values of Y may not be available. In such cases, the degree of deviation can be inferred using Δ_X and/or the (observed and historical) values of X . Since the response object contains requested measurements, such estimation is arguably feasible considering the contents of the node (e.g., array/object referencing, mathematical expression, etc.) and the concept of tainted data propagation implemented in our generated graph.

According to these observations and representations, we develop a set of local patterns listed in Table I. Each pattern is formatted as $LPTN_k \equiv \langle F/S/Others, ED/UED/\top \rangle$, where F , S , and $Others$ represent the float-type node, string-type node, and others node (e.g., function call, object), respectively. In addition, the expected deviation and the unexpected deviation are denoted as ED and UED , respectively. Moreover, in a few cases, the degree of deviation may not exist (considering different variants of code structures) and may not be applicable (function call). To handle such nodes, we use a new notation \top (top).

IV. CASE STUDY

In this case study, we utilize a public DERMS application program repository¹ to evaluate the feasibility of our

¹https://github.com/GRIDAPPSD/gridapssd-soap-server/blob/master/soapServer/soap_server.py

proposed techniques. In the codebase, there are several crucial virtual physical variables: `equipment_id4dispatch`, `equipment_name`, `equipment_p`, `equipment_q`, `equipment_p_meas`, `equipment_q_meas`, `equipment_maxIFault`, `equipment_ratedS`, `equipment_ratedU`, and `equipment_type`. These variables represent the unique ID, name, expected active power, expected reactive power, measured active power, measured reactive power, maximum fault current, rated apparent power (the maximum power capacity under normal conditions), rated apparent voltage, and the type of each of equipment, respectively. After analyzing the application program, a set of event types is generated (referred to Table II). It should be noted that whereas the italic font (*E*) used in the table represents an event type, the non-italic font (E) used in the analysis represents an event instance.

For each failure incident, a sequence of events can be extracted from the corresponding log files. At the beginning of the analysis, the analyst can utilize this sequence to find the specific tainted path(s) in the dependency graph and ignore the unrelated ones. After that, the analyst goes through every node in that path and searches for matched patterns. Finally, a decision on the root cause is made based on the pattern-matching results.

The following case studies show the practical use of this approach. The corresponding sequence of synthesized events is stored in CSV format and can be found in our dataset repository². The CSV files are ‘events_seq_1’, ‘events_seq_2’, ‘events_seq_3’, and ‘events_seq_4’, representing the event sequences for the four case studies, aligned with their respective order. Each row in these CSV files represents an event instance, and the four columns denote the ID, type, recorded value, and description of the instance, respectively. For example, the row 2, E1, 1972301.79, ‘magnitude’ sensing event represents an instance of type E1, corresponding to a magnitude sensing event with the value 1972301.79. We generated the synthesized events based on how such events are identified in the real world. It should be noted that events related to PMU measurements are collected from IEEE C37.118 direct capture files, network events are extracted from the relevant data fields of the PCAP (packet capture) file, and cyberspace events are collected from the corresponding DERMS application logs, which are usually saved as a TXT file.

Case 1. Consider a scenario in which equipment functions unexpectedly and significant discrepancies in their power measurements are monitored. Consequently, some equipment has been damaged, and an excessive efficiency loss is observed in the power system. In the ground truth, inconsistency is observed in the field measurements due to a system fault, and an ADS has detected something abnormal.

To investigate the cause of the system failure, a security analyst is assigned. After preliminary evaluation of the incident report, he finds that the “angle” and “magnitude” values of one equipment are inconsistent. Therefore, he

TABLE II
THE EVENT TYPES USED IN OUR CASE STUDIES

#	Description
<i>E1</i>	a DER device or a virtual physical variable is found abnormal by an ADS
<i>E2</i>	<code>response_obj</code> is consistent
<i>E3</i>	values in one or more fields of <code>response_obj</code> are inconsistent
<i>E4</i>	conditional check is passed
<i>E5</i>	corresponding virtual physical variables are manipulated
<i>E6</i>	‘ <code>equipment_p_meas</code> ’ is consistent
<i>E7</i>	‘ <code>equipment_q_meas</code> ’ is consistent
<i>E8</i>	relevant intermediate mathematical calculations are inconsistent
<i>E9</i>	no manipulation in the mathematical calculations
<i>E10</i>	‘ <code>forward_value</code> ’ is inconsistent
<i>E11</i>	‘ <code>reverse_value</code> ’ is inconsistent
<i>E12</i>	active and reactive powers are consistent
<i>E13</i>	corresponding difference messages are altered
<i>E14</i>	corresponding difference messages are consistent
<i>E15</i>	‘ <code>message</code> ’ containing unexpected values is sent to the physical side

looks into the codebase to get the appropriate program variable(s). Since only `equipment_p_meas` and `equipment_q_meas` are the virtual physical variables related to these measurements, the security specialist generates a dependency graph starting from these two variables according to the technique proposed in Section III-C. After initial generation of the upper subgraph (USG), two potential sources `GridAPPSD(username, password)` and `conn.get_response(t.TIMESERIES, message)` are found using Heuristic at Section III-C. Then, the lower subgraph (LSG) is constructed using a forward tracking strategy that halts at the sink `conn.send(input_topic, message)`. After that, the graph simplification algorithm is applied, which deducts 16 nodes from the original graph ($57 \rightarrow 41$), achieving 28.07% node reduction. The final graph is illustrated in Figure 7. For simplicity of further analysis, some intermediate nodes are skipped in the USG, and node numbering is started from the API request `conn.get_response(t.TIMESERIES, message)`. Here, nodes in the USG and LSG are colored blue and red, respectively. In addition, the virtual physical variables, sources, and sinks are represented with yellow-colored nodes.

After pruning the dependency graph, the analyst uses the recorded sequence of events and his domain knowledge to identify the specific tainted path related to the incident. According to Table I, the analyst figures out that the subpath $N_{12} \rightarrow N_{13} \rightarrow N_{15} \rightarrow N_{17} \rightarrow N_{19}$ is not related to the incident. So, these nodes are not explored during further analysis. Next, each node along the related path is traversed to match a set of patterns based on the strategies described in Section III-D.

From ‘events_seq_1’ file of the dataset, “angle” and “magnitude” of the PMU measurement are 25.345 and 1972301.79, respectively (the sensing events). Besides, identical values are observed in the network packet as well as in the application log (network packet message event and response object, respectively). Based on this observation, the analyst generates two histograms to monitor whether these values are deviated from the ‘benign’ ones or not. According to Figures 8a and 8b, the observed angle can be allocated to the leftmost bin; whereas, the magnitude cannot be assigned to any of them. Therefore, it is clear that *deviation* exists in the PMU measurement, which matches with the global pattern

²<https://github.com/MdShamim097/Dataset-Events-Sequence.git>



Fig. 7. Dependency graph for case study.

$GPTN_5 \equiv \langle C_{dn}, C_{na}, Y \rangle$ and the matched event instance is E1. In particular, the histograms are generated using a log collected from the National Renewable Energy Laboratory (NREL) that contains ‘benign’ values of all essential measurements. After that, the analyst continues exploring the selected path and looks for potential matches of local patterns. The first node in the graph is a function call, whose corresponding pattern is $LPTN_5$. The next node is the response object, where the global pattern was found. Based on the observed values, the *deviation* at this node can be considered as high (H). Since measurement information is carried from node N_2 to N_9 , their executed values are arguably available in the application log. In addition, the observed deviations are as expected, that is $\Delta_X \rightarrow \Delta_Y$ since no program memory is corrupted. Thus, the matched patterns are $LPTN_1 \equiv \langle F, ED \rangle$, and these patterns represent the occurrence of event instance E5. Notably, even if any log is not available, for example *startYvalue*, Δ_Y can be estimated because of their simple relations and code structures. However, from *Yvalue_start* (node N_{10}) to *nominalyvalues[i_equip]* (node N_{16}), logs are not available as they carry mathematical calculations. Although the analyst may try to estimate their values, it is not always possible due to their complex dependency. So, the deviations for these nodes are taken as unknown (pattern: $LPTN_4$). Importantly, such uncertainty of values does not affect the analysis even if any malicious activities take place within these nodes (e.g., memory corruption), because the contaminated values will ultimately propagate through the subsequent nodes to the end. After *nominalyvalues[i_equip]*, next related node is *forward_value*. Since it contains the

measured active power value, its historical logs are certainly available, and the degree of deviation can be obtained using the histogram approach. In this case, the deviation found is *ED* (pattern, $LPTN_1 \equiv \langle F, ED \rangle$) since no memory corruption has occurred. In addition, since the deviations exist at this node, event instance E10 is matched. The next node is an object (*DifferenceMessage*), which is matched with $LPTN_5$ according to the definition. Other nodes, especially from N_{21} to N_{25} , are related to dispatching. So, their logs are always available, and the corresponding Δ_Y can be easily calculated. Consequently, the deviation shows $\Delta_X \rightarrow \Delta_Y$ characteristics, which indicate the event instances E13 and E15, and matches pattern $LPTN_1 \equiv \langle S, ED \rangle$. In this way, E1 → E3 → E5 → E10 → E13 → E15 is observed as the sequence of event instances for this failure incident.

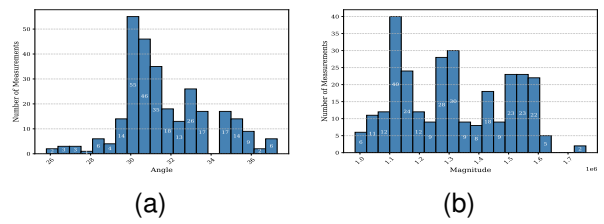


Fig. 8. Histograms of (a) angle and (b) magnitude of the equipment

After getting the pattern matching results, the analyst makes the final reasoning as follows: first, only one global pattern is found. Then, it is propagated through the program according to the deviation that is expected. In addition, no unexpected deviation is observed during the analysis. Therefore, the

analyst can conclude that a system fault is the most likely root cause of the system failure. In this way, our proposed graph construction and pattern matching techniques facilitate the task of distinguishing system faults and cyberattacks in the CPS domain, especially in DER systems. The synthesized reasoning is shown in Table III.

Case 2. In this test case, an FDI attack is treated as the ground truth of system failure, and the corresponding recorded event sequence is shown in the ‘events_seq_2’ file. Using this sequence, the analyst proceeds with the related tainted path. In this case, the “angle” and “magnitude” of the field measurements are found to be 30.7597 and 1156739.528, respectively. On the other hand, 30.7597 and 1430307.59 are found in the corresponding network packet and application log. From these values, it is clear that $v_x^d \neq v_x^n$ and $v_x^n = v_x^a$, which indicates the possibility of a suspicious act on the communication side. From the histograms illustrated in Figures 8a and 8b, the observed “angle” can be allocated to one of the largest bins (not deviated much). However, the “magnitude” is tracked to the twelfth bin, which can be considered as *moderate deviation* (M). Thus, the analyst identifies $GPTN_1 \equiv \langle I_{dn}, C_{na}, Y \rangle$ as the global pattern and $LPTN_1 \equiv \langle F, ED \rangle$ as the local pattern (for node N_1). Regarding the analysis in the local region (application program), the matched patterns are similar to test case 1, as no direct interruption (e.g., memory corruption) takes place in the program region. However, the degree of deviations in the dependent nodes (Δ_X, Δ_Y) is different since this time $\Delta_X = M$ for the first node (response object), rather than $\Delta_X = H$. Although the observed sequence is similar to the previous test case, they represent different event instances and hence different incidents. Importantly, the matched global pattern plays a significant role in differentiating the root causes. All the matched patterns are shown in Table III.

Case 3. The ground truth for this test case is a memory corruption attack, where the attacker has manipulated one of the memory locations to change the reactive power measurements. According to the recorded sequence in the ‘events_seq_3’ file, and the histograms in Figures 8a and 8b, *no deviation* is found in these values, matching the global pattern $GPTN_4 \equiv \langle C_{dn}, C_{na}, N \rangle$. After initial selection based on the sequence of recorded events and based on domain knowledge, the analyst suspects the subpath $N_{12} \rightarrow N_{13} \rightarrow N_{15} \rightarrow N_{17} \rightarrow N_{19}$ to be manipulated. So, he avoids analyzing the nodes $N_{12} \rightarrow N_{14} \rightarrow N_{16} \rightarrow N_{18} \rightarrow N_{19}$, and continues matching patterns in the selected path. At node N_1 (the response object), the pattern is $LPTN_1 \equiv \langle F, ED \rangle$. Importantly, here $\Delta = 0$ since no deviation was observed during the global analysis, the event instance is E2. In the following nodes from N_2 to N_9 , the same patterns $LPTN_1$ are found with $\Delta_X(= 0) \rightarrow \Delta_Y(= 0)$, which is expected and the found event instances are E6 and E7. However, at node N_{17} containing `reverse_value`, an unexpected deviation ($\Delta_X \rightarrow \Delta'_Y$) is observed (see 11th item in Table III), which indicates an occurrence of manipulation at this node or any of its predecessors on which this node has data dependency. Thus, the matched pattern is

$LPTN_2 \equiv \langle F, UED \rangle$ and the corresponding matched event instance is E11. Since nodes $N_{19} - N_{20}$ and $N_{22} - N_{25}$ have data dependency with node N_{17} , their values are also unexpectedly changed. However, the matched patterns are $LPTN_3 \equiv \langle S, UED \rangle$ as these nodes contain string-typed values. Therefore, the observed event sequence in this case is: E1→E2→E6→E7→E11→E13→E15. Finally, reasoning can be done as follows: no deviation is found in the global region, but several unexpected deviations are observed in the local region (application program), which is a prominent indicator of a memory corruption attack. Therefore, the analyst can conclude a memory corruption is the root cause of system failure.

Case 4. In this test, the ground truth is also a memory corruption attack; but, the attack takes place in any of the intermediate nodes, where mathematical calculations are manipulated to alter the active power measurements. Specifically, the observed values in the field measurements, network packet, and application log are 36.173 and 1243590.094, respectively (see first four items in the ‘events_seq_4’ file). Since these values remain consistent on both physical and cyber sides, the analyst further checks for potential deviations and their degrees. According to the histograms in Figures 8a and 8b, both values are located in two considerably moderate bins. Thus, *deviation* (especially, M) may exist, which matches the global pattern $GPTN_5 \equiv \langle C_{dn}, C_{na}, Y \rangle$. According to the recorded events sequence in Table IV, the analyst selects the subpath $N_{12} \rightarrow N_{14} \rightarrow N_{16} \rightarrow N_{18} \rightarrow N_{19}$, and neglects the opposite one. In the local region, the patterns up to node N_{16} are exactly identical to the previous test (case 3), except Δ_X and Δ_Y are not 0 since deviation (expected or unexpected) is observed both in global and local portions. However, at node N_{18} , deviation is observed in the active power value while comparing the histogram of ‘benign’ values. This indicates that memory corruption has occurred either at this node or any of the previous intermediate nodes. Consequently, the subsequent dependent nodes $N_{19}, N_{22}, N_{23}, N_{24}$, and N_{25} are also deviated. Regarding the event sequence, E1→E3→E5→E10→E13→E15 is matched, which verifies the detection of related event instances. Interestingly, though the event sequence filters out the unrelated tainted path in the same way as in the previous case, they are substantially different and represent separate incidents. During the final reasoning, two major observations can be made: first, the matched global pattern indicates a slight deviation in response-related values; second, some expected and unexpected deviations are observed in the program region. Since alternation in the program side strongly justifies a memory corruption attack and the observed deviation in the global part does not necessarily indicate a system fault or FDI, the analyst can conclude memory corruption as the root cause of the system failure.

Concluding Remarks. The conducted test cases bear clear testimony to the effectiveness of our proposed approach. Although all test cases reflect the significance of the co-existence of global and local patterns, each conveys

a distinctive implication. More specifically, the first two cases emphasize the necessity of global patterns, especially how they effectively capture the distinct characteristics of individual causes. On the other hand, the importance of local patterns is demonstrated in the last two test cases. Notably, the fourth case demonstrates the necessity of this type of pattern to make the appropriate decision even when the matched global pattern indicates something else. In this way, the proposed approach of differentiating undetected faults and cyberattacks becomes more rigorous and credible.

TABLE III
TEST CASE ANALYSIS

#	Pattern Matching Results	Nodes and Reasoning	Matched Sequence	Conclusion
1	Global Patterns: No $GPTN_1$ or $GPTN_2$ No $GPTN_3$ or $GPTN_4$ No $GPTN_7$ or $GPTN_8$ Local Patterns: No $LPTN_1$ or $LPTN_2$ No $LPTN_3$ or $LPTN_4$ Some $LPTN_1$ and $LPTN_2$ (nothing abnormal)	$N_1: GPTN_1$ (root cause; object itself; practically first node) $N_2 - N_6: LPTN_1$ (response object related; $\Delta \neq 0$) $N_{10} - N_{12}: N_1, N_4, N_7, N_8$ (log not available; hard to estimate) $N_{18} - N_{20}: N_1, N_2, N_3, N_4$ (log not available; hard to estimate) $N_{19}: LPTN_5$ (not applicable; object name) $N_{20}, N_{21}: LPTN_6$ (not applicable; function call)	$E1 \rightarrow^1 E3 \rightarrow E5 \rightarrow E10 \rightarrow E13 \rightarrow E15$	System Fault
2	Global Patterns: No $GPTN_3$ or $GPTN_4$ No $GPTN_7$ or $GPTN_8$ Local Patterns: One $LPTN_1$ No $LPTN_2$ or $LPTN_3$ Some $LPTN_1$ and $LPTN_3$	$N_1: GPTN_3$ $N_2 - N_6: LPTN_1$ ($\Delta \neq 0$) $N_{10} - N_{12}, N_4, N_6: LPTN_4$ $N_{18} - N_{20}: N_1, N_2, N_3, N_4$ $N_{19}: LPTN_5$ $N_{20}, N_{21}: LPTN_6$	$E1 \rightarrow^2 E3 \rightarrow E5 \rightarrow E10 \rightarrow E13 \rightarrow E15$	FDI
3	Global Patterns: No $GPTN_1$ or $GPTN_2$ No $GPTN_3$ or $GPTN_4$ No $GPTN_7$ or $GPTN_8$ Local Patterns: One $LPTN_1$ Multiple $LPTN_2$ Some $LPTN_1$ and $LPTN_2$	$N_1: GPTN_1$ $N_2 - N_6: LPTN_1$ ($\Delta = 0$) $N_{10} - N_{13}, N_4, N_6: LPTN_4$ $N_{17}: LPTN_2$ (dispatch related; unexpected) $N_{18} - N_{20}: N_1, N_2, N_3, N_4$ $N_{19}: LPTN_5$ $N_{21}: LPTN_1$ (dispatch related; expected) $N_{22}, N_{23}: LPTN_6$	$E1 \rightarrow E2 \rightarrow E6 \rightarrow E7 \rightarrow E11 \rightarrow E13 \rightarrow E15$	Memory Corruption
4	Global Patterns: No $GPTN_1$ or $GPTN_2$ No $GPTN_3$ or $GPTN_4$ No $GPTN_7$ or $GPTN_8$ Local Patterns: One $LPTN_1$ Multiple $LPTN_2$ Some $LPTN_1$ and $LPTN_2$	$N_1: GPTN_1$ $N_2 - N_6: LPTN_1$ ($\Delta \neq 0$) $N_{10} - N_{13}, N_4, N_6: LPTN_4$ $N_{18}: LPTN_2$ $N_{21} - N_{23}: LPTN_3$ (dispatch related; unexpected) $N_{19}: LPTN_5$ $N_{20}: LPTN_1$ (dispatch related; unexpected) $N_{22}, N_{23}: LPTN_6$	$E1 \rightarrow E3 \rightarrow E5 \rightarrow E10 \rightarrow E13 \rightarrow E15$	Memory Corruption

Comments on Benchmark Evaluation. Since existing works do not integrate physical side measurements and cyberspace information, no appropriate baseline is available to compare. Nevertheless, it should be noticed that the pattern matching mechanism can be scaled to a large-scale evaluation benchmark where a large number of recorded sequences of events are available. Using such a benchmark, performance metrics such as accuracy and F1 scores can be quantitatively measured. In our future work, we would collaborate with a DER industry partner and develop such a benchmark.

V. CONCLUSION

This paper introduces the first combined analysis of physical measurements and cyberspace information to differentiate faults and cyberattacks in DER systems. In particular, a non-trivial taint analysis technique is proposed to efficiently capture the propagation of untrusted data in DER application programs, along with devising a set of patterns to bridge the semantic gap between cyber and physical sides. During analysis, the generated graph is traversed to match a set of patterns, and the decision on the root cause of system failure is made based on the pattern-matching results. One future work is to make the reasoning of the pattern-matching results more automatic.

REFERENCES

- [1] M. S. Ahsan, H. Wang, V. R. Motakatla, M. Zhu, and P. Liu, “Simplifying taint-style dependency graphs generated from DERMS application program,” Penn State Cyber Security Lab, Pennsylvania, USA, Tech. Rep. CSL-2025-001, September 2025, [Online]. Available: <https://s2.ist.psu.edu/TechReport-graph-simplification.pdf>.
- [2] M. K. Alam, F. Khan, J. Johnson, and J. Flicker, “A comprehensive review of catastrophic faults in pv arrays: types, detection, and mitigation techniques,” *IEEE Journal of Photovoltaics*, vol. 5, no. 3, pp. 982–997, 2015.
- [3] America’s Cyber Defense Agency, “IRGC-Affiliated Cyber Actors Exploit PLCs in Multiple Sectors, Including US Water and Wastewater Systems Facilities,” <https://www.cisa.gov/news-events/cybersecurity-advisories/aa23-335a>, accessed: 13 January, 2025.
- [4] S. Amini, F. Pasqualetti, M. Abbaszadeh, and H. Mohsenian-Rad, “Hierarchical location identification of destabilizing faults and attacks in power systems: A frequency-domain approach,” *IEEE Transactions on Smart Grid*, vol. 10, no. 2, pp. 2036–2045, 2017.
- [5] W. Ao, Y. Song, and C. Wen, “Adaptive cyber-physical system attack detection and reconstruction with application to power systems,” *IET Control Theory & Applications*, vol. 10, no. 12, pp. 1458–1468, 2016.
- [6] S. Arzt, S. Rasthofer, C. Fritz, E. Bodden, A. Bartel, J. Klein, Y. Le Traon, D. Oeteau, and P. McDaniel, “Flowdroid: Precise context, flow, field, object-sensitive and lifecycle-aware taint analysis for android apps,” *ACM sigplan notices*, vol. 49, no. 6, pp. 259–269, 2014.
- [7] O. A. Beg, L. V. Nguyen, T. T. Johnson, and A. Davoudi, “Cyber-physical anomaly detection in microgrids using time-frequency logic formalism,” *IEEE Access*, vol. 9, pp. 20012–20021, 2021.
- [8] M. Benninger, M. Hofmann, and M. Liebschner, “Anomaly detection by comparing photovoltaic systems with machine learning methods,” in *NEIS 2020; Conference on Sustainable Energy Supply and Energy Storage Systems*. VDE, 2020, pp. 1–6.
- [9] M. Ganjkhani, M. Gilanifar, J. Giraldo, and M. Parvania, “Integrated cyber and physical anomaly location and classification in power distribution systems,” *IEEE Transactions on Industrial Informatics*, vol. 17, no. 10, pp. 7040–7049, 2021.
- [10] K. Gupta, S. Sahoo, R. Mohanty, B. K. Panigrahi, and F. Blaabjerg, “Distinguishing between cyber attacks and faults in power electronic systems—a noninvasive approach,” *IEEE Journal of Emerging and Selected Topics in Power Electronics*, vol. 11, no. 2, pp. 1578–1588, 2022.
- [11] G. Liang, S. R. Weller, J. Zhao, F. Luo, and Z. Y. Dong, “The 2015 ukraine blackout: Implications for false data injection attacks,” *IEEE transactions on power systems*, vol. 32, no. 4, pp. 3317–3318, 2016.
- [12] S. Madabhushi and R. Dewri, “A survey of anomaly detection methods for power grids,” *International Journal of Information Security*, vol. 22, no. 6, pp. 1799–1832, 2023.
- [13] Y. Mo, T. H.-J. Kim, K. Brancik, D. Dickinson, H. Lee, A. Perrig, and B. Sinopoli, “Cyber-physical security of a smart grid infrastructure,” *Proceedings of the IEEE*, vol. 100, no. 1, pp. 195–209, 2011.
- [14] S. Sahoo, Y. Yang, and F. Blaabjerg, “Resilient synchronization strategy for ac microgrids under cyber attacks,” *IEEE Transactions on Power Electronics*, vol. 36, no. 1, pp. 73–77, 2020.
- [15] J. Sakhnini, H. Karimipour, A. Dehghaniantha, and R. M. Parizi, “Physical layer attack identification and localization in cyber-physical grid: An ensemble deep learning based approach,” *Physical Communication*, vol. 47, p. 101394, 2021.
- [16] Y. Shen and Z. Qin, “Detection, differentiation and localization of replay attack and false data injection attack based on random matrix,” *Scientific Reports*, vol. 14, no. 1, p. 2758, 2024.
- [17] M. Sridharan, S. Artzi, M. Pistoia, S. Guarneri, O. Tripp, and R. Berg, “F4f: taint analysis of framework-based web applications,” in *Proceedings of the 2011 ACM international conference on Object oriented programming systems languages and applications*, 2011, pp. 1053–1068.
- [18] M. Syfert, A. Ordys, J. M. Kościelny, P. Wnuk, J. Możaryn, and K. Kukielka, “Integrated approach to diagnostics of failures and cyber-attacks in industrial control systems,” *Energies*, vol. 15, no. 17, p. 6212, 2022.
- [19] G. Tertychny, N. Nicolaou, and M. K. Michael, “Classifying network abnormalities into faults and attacks in iot-based cyber physical systems using machine learning,” *Microprocessors and Microsystems*, vol. 77, p. 103121, 2020.
- [20] C.-W. Tsai, C.-W. Yang, F.-L. Hsu, H.-M. Tang, N.-C. Fan, and C.-Y. Lin, “Anomaly detection mechanism for solar generation using semi-supervision learning model,” in *2020 Indo-Taiwan 2nd International Conference on Computing, Analytics and Networks (Indo-Taiwan ICAN)*. IEEE, 2020, pp. 9–13.
- [21] Q. Wang, K. Paynabar, and M. Pacella, “Online automatic anomaly detection for photovoltaic systems using thermography imaging and low rank matrix decomposition,” *Journal of quality technology*, vol. 54, no. 5, pp. 503–516, 2022.
- [22] Y. Zhao, B. Lehman, J.-F. de Palma, J. Mosesian, and R. Lyons, “Fault analysis in solar pv arrays under: Low irradiance conditions and reverse connections,” in *2011 37th IEEE Photovoltaic Specialists Conference*. IEEE, 2011, pp. 002000–002005.